10/11/12/96 JS (1)

SANDIA REPORT

SAND96-8580 • UC–401
Unlimited Release
Printed August 1996

Aspects of Nitrogen Surface Chemistry Relevant to TiN Chemical Vapor Deposition

M. T. Schulberg, M. D. Allendorf, D. A. Outka

Prepared by
Sandia National Laboratories
Albuquerque, New Mexico 87185 and Livermore, California 94551
for the United States Department of Energy
under Contract DE-AC04-94AL85000

Approved for public release; distribution is unlimited.

MASTER

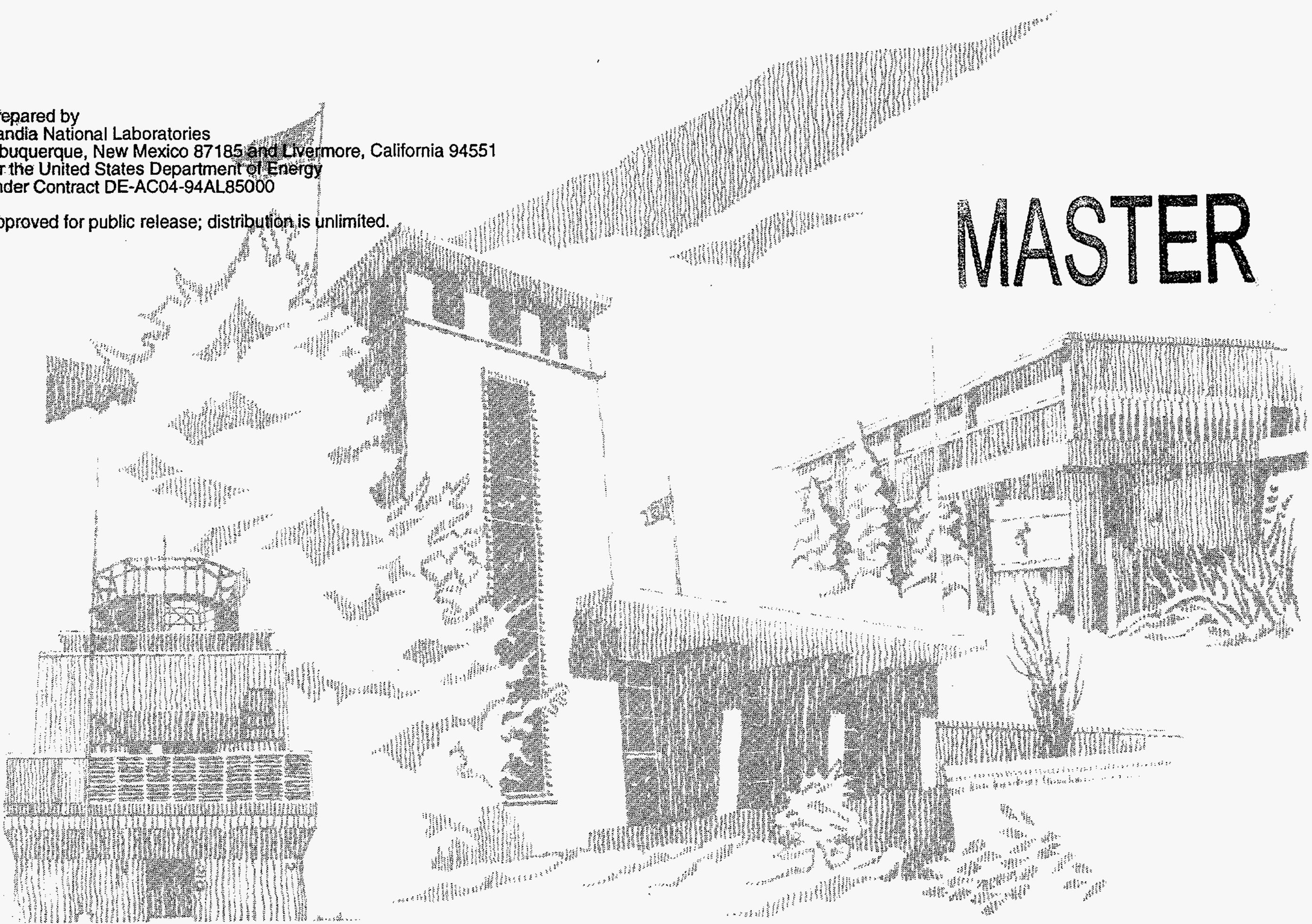

SF2900Q(8-81)

DISTRIBUTION OF THIS DOCUMENT IS UNLIMITED

Issued by Sandia National Laboratories, operated for the United States Department of Energy by Sandia Corporation.
NOTICE: This report was prepared as an account of work sponsored by an agency of the United States Government. Neither the United States Government nor any agency thereof, nor any of their employees, nor any of the contractors, subcontractors, or their employees, makes any warranty, express or implied, or assumes any legal liability or responsibility for the accuracy, completeness, or usefulness of any information, apparatus, product, or process disclosed, or represents that its use would not infringe privately owned rights. Reference herein to any specific commercial product, process, or service by trade name, trademark, manufacturer, or otherwise, does not necessarily constitute or imply its endorsement, recommendation, or favoring by the United States Government, any agency thereof or any of their contractors or subconractors. The views and opinions expressed herein do not necessarily state or reflect those of the United States Government, any agency thereof or any of their contractors or subcontractors.

This report has been reproduced from the best available copy.

Available to DOE and DOE contractors from:

Office of Scientific and Technical Information
P. O. Box 62
Oak Ridge, TN 37831

Prices available from (615) 576-8401, FTS 626-8401

Available to the public from:

National Technical Information Service
U.S. Department of Commerce
5285 Port Royal Rd.
Springfield, VA 22161

DISCLAIMER

Portions of this document may be illegible in electronic image products. Images are produced from the best available original document.

UC-401

SAND96-8580
Unlimited Release
Printed August 1996

ASPECTS OF NITROGEN SURFACE CHEMISTRY RELEVANT TO TiN CHEMICAL VAPOR DEPOSITION

Michelle T. Schulberg,[a] Mark D. Allendorf,[b] and Duane A. Outka[c]
Sandia National Laboratories, Livermore, CA 94551

ABSTRACT

NH_3 is an important component of many chemical vapor deposition (CVD) processes for TiN films, which are used for diffusion barriers and other applications in microelectronic circuits. In this study, the interaction of NH_3 with TiN surfaces is examined with temperature programmed desorption (TPD) and Auger electron spectroscopy. NH_3 has two adsorption states on TiN: a chemisorbed state and a multilayer state. A new method for analyzing TPD spectra in systems with slow pumping speeds yields activation energies for desorption for the two states of 24 kcal/mol and 7.3 kcal/mol, respectively. The sticking probability into the chemisorption state is ~0.06. These results are discussed in the context of TiN CVD. In addition, the high temperature stability of TiN is investigated. TiN decomposes to its elements only after heating to 1300 K, showing that decomposition is unlikely to occur under CVD conditions.

[a] Present address: Varian Associates, Palo Alto, CA 94304.
[b] Author to whom correspondence should be addressed. mdallen@sandia.gov.
[c] Present address: Lam Research Corporation, Fremont, CA 94538.

INTRODUCTION

Titanium nitride's unique combination of mechanical, chemical, optical, and electronic properties leads to many thin-film applications for integrated circuits. The most widely-discussed use for TiN is as a diffusion barrier, but it can also serve to prevent the attack of WF_6 on Si during W chemical vapor deposition (CVD),[1] as a nucleation layer between intermetal-level dielectrics and CVD tungsten,[2] and as a gate electrode in MOS integrated circuits.[3] For all of these applications, as feature sizes shrink and aspect ratios grow, the issue of good step coverage becomes increasingly important. It is therefore essential to manufacture conformal coatings of TiN.

CVD is the best way to produce conformal coatings of the quality required for ULSI applications. Both inorganic and metalorganic TiN CVD processes have been developed. The most common inorganic precursor[4,5,6,7] is $TiCl_4$ and the typical metalorganic precursors[1,8,9,10] are tetrakis-dimethylamidotitanium ($Ti(NMe_2)_4$, TDMAT) and tetrakis-diethylamidotitanium ($Ti(NEt_2)_4$, TDEAT). Excess NH_3 is usually the nitrogen source for inorganic deposition processes. In the case of the metalorganic precursors, an additional nitrogen-containing reactant is not stoichiometrically required; however, an excess of NH_3 is necessary to produce high-purity, low-resistivity films.[11] Also, for TDMAT, it has been shown[9] that when NH_3 is present, the nitrogen in the film comes from NH_3 and not from the metalorganic compound. The overall deposition reaction is then the same in all cases:

$$6TiX_4 + 8NH_3 \rightarrow 6TiN + 24HX + N_2 \qquad X = Cl,\ NMe_2,\ NEt_2 \qquad (1)$$

NH_3 therefore plays a prominent role in the deposition process, by means of either gas-phase or surface reactions or both. To this point, the gas-phase chemistry has been studied in more depth than the surface reactions. TDMAT and NH_3 undergo a gas-phase transamination reaction,[12,13] with dimethylamine as the only clearly identified product. On the other hand, $TiCl_4$ and NH_3 form complexes with each other[14,15,16,17,18] at temperatures below ~523 K.[4] In the only previous surface study, Truong et al.[19] speculated that adsorbed NH_x species could react with adsorbed TDMAT at low pressures ($<10^{-4}$ torr) to produce low-carbon films. They also briefly examined the reaction of NH_3 on TiN_x surfaces, but the results were not fully analyzed. In order to further clarify the role of surface processes involving NH_3 in TiN CVD, a more detailed investigation of the adsorption and desorption kinetics of NH_3 on TiN is presented here.

Desorption of NH_3 from a variety of metal and semiconductor surfaces has been studied previously. Temperature programmed desorption (TPD) spectra from Pt,[20,21,22] Ru(001),[23] Mo(100),[24] MoN,[25] Ni(110),[26] NiO(100),[27] Ag(311),[28] GaAs(100),[29,30,31] Si(100),[32,33] TiO_2,[34] and TiN_x[19] generally share two characteristics: 1) multiple desorption features, which often overlap, and 2) broad peaks, ending with a long tail on the high temperature side. The multiple desorption features represent four different types of NH_3 adsorption, distinguished by the strength of the adsorbate-surface interaction. The molecules desorbing at the highest temperatures, i.e., with the strongest interaction with the surface, are produced by the recombination of dissociatively adsorbed species, in which a N-H bond has broken and both fragments have bonded to the surface. In addition, three molecular adsorption states have been described. In decreasing order of desorption temperature, these are: chemisorption, physisorption, and multilayer or solid NH_3. The chemisorbed NH_3 molecules do not dissociate, yet still form a strong bond to the surface. The

physisorbed molecules are attracted to the surface more weakly, but in contrast to the multilayer they interact directly with the substrate. Finally, when the sample temperature is below ~200 K, a thick layer of solid NH_3 can form. Since the chemisorption state often saturates at coverages well below 1 monolayer (ML), the physisorption state can be envisioned as the first layer of solid NH_3 bound to bare regions of the substrate. Each substrate from which NH_3 TPD spectra have been obtained displays its own combination of the four processes, creating complex desorption spectra.

All of the NH_3 TPD spectra display a long tail, which is due to the slow pumping speed of NH_3 in stainless-steel vacuum chambers. NH_3 that has desorbed from the sample may readsorb on the chamber walls, then desorb at some later time to be detected by the mass spectrometer. It is difficult to extract accurate desorption parameters from these distorted peaks since Redhead analysis[35] assumes essentially infinite pumping speeds. The activation energy for desorption can be estimated from the peak desorption temperature, but none of the previous NH_3 TPD studies included an analysis of coverage-dependence or a full fit to the experimental data. In this work, the finite pumping speed of NH_3 is accommodated by introducing a new parameter to the fitting routine. The characteristic pumping time of the vacuum system, τ, is defined by Redhead as the ratio of the volume of the chamber to the pumping speed. With the incorporation of this additional parameter, the shape of the experimental curves is reproduced and the activation energy and initial surface coverage can be calculated.

Finally, the thermal stability of TiN is investigated. Since TiN CVD takes place at elevated temperatures (450-1000 K), it is important to understand the film's behavior under these conditions. Also, its ability to withstand high temperatures has implications for TiN used in wear- and corrosion-resistant coatings. One question that can be addressed by UHV analytical techniques is the temperature-dependent rate of TiN decomposition. Entropy considerations dictate that at high temperatures, TiN should be unstable with respect to dissociation to Ti and N_2. The desorption of N_2 from the TiN surface is also important since Equation 1 suggests that N_2 is a product of the deposition reaction, as required to balance the formal reduction in the oxidation state of the titanium from +4 to +3; however, evolution of N_2 has not been documented. There are no obvious gas-phase pathways for producing N_2, so it has generally been assumed that N_2 is produced via a surface reaction.[36] Thermodynamic calculations[37] predict Ti-N bond strengths for gas-phase compounds in the range of 85-100 kcal/mol, suggesting that N_2 desorption from a TiN surface is too slow to contribute to processes at typical CVD temperatures. In order to verify these calculations, the bond strength of nitrogen to the TiN surface is examined using TPD and Auger electron spectroscopy (AES).

EXPERIMENTAL TECHNIQUE

The experiments were performed in a vacuum chamber that has been described previously,[38,39] modified such that the chamber housing the mass spectrometer was pumped by a turbomolecular pump rather than by an ion pump. The TiN samples (Goodfellow Corp.) were sputter-deposited films 2-3 μm thick on 8-mm-diameter Ti disks. Tantalum tabs held the sample to a Mo "button" heater at the end of a liquid-N_2 cryostat. The temperature was measured by a chromel-alumel thermocouple wedged under one of the tabs.

When first installed in the vacuum chamber, the TiN films were coated with a thick oxide layer. Following repeated cycles of sputtering with 5-keV Ar^+ ions and annealing at 900 K, AES showed that C and O were the main contaminants, with typical C/Ti and O/Ti atomic ratios of <0.2 and <0.1 respectively. Unfortunately, the Ti/N ratio could not be determined by AES since the N Auger peak at 390 eV overlaps with a Ti peak[40] and a standard of known composition was not available. Changes in the AES peak shapes did, however, serve as a diagnostic for depletion of N from the film following extended sputtering cycles. The depletion was confirmed by a change in the film's color from gold to silver. When this occurred, a new sample was installed.

Before each TPD experiment, the film was sputter-cleaned for 15 minutes and then annealed for 5 minutes. NH_3 was admitted through a stainless-steel dosing tube, raising the chamber pressure to roughly 10^{-9} to 10^{-8} torr. The sample temperature was held at 100 K during exposure to NH_3 and then raised to 850 K at 5 K/s while a TPD spectrum was recorded by the differentially-pumped mass spectrometer. Three different dosing arrangements were used. For some experiments, the sample was turned away from the doser so that the incident flux could be estimated from the chamber pressure integrated over the exposure time. The sticking probability could then be calculated by comparing the incident flux to the integrated desorption signal during the TPD ramp. Unfortunately, this arrangement led to high background levels of NH_3 in the vacuum chamber, which further aggravated the pumping speed problem. To obtain cleaner TPD spectra when measurement of the incident flux was not required, the sample was placed directly in front of the doser during the exposure, minimizing adsorption of NH_3 on the chamber walls. Under these conditions, however, it was difficult to limit the exposure to obtain low coverage spectra. To further reduce the NH_3 background and to provide better control of the magnitude of the exposure, in some cases the NH_3 was diluted with Ar in a ratio of ~1:3 and the sample was then placed directly in front of the dosing tube.

Additional measurements of the sticking probability were made using the directed-beam doser technique described by Dresser et al.[33] NH_3 was introduced through the doser with the sample facing away from the beam. The chamber pressure was recorded while the sample was rotated into the path of the beam and then later rotated back out. Finally the doser valve was closed. Sharp pressure changes were not achieved, due to adsorption and desorption on the walls of the stainless-steel doser tubing, but qualitative results could be evaluated.

For studies of thermal decomposition, the same TiN samples were clamped onto a resistively-heated 0.003"-thick Mo support. A W/5% Re:W/26% Re thermocouple was spot-welded to the Mo support near the sample. The TiN surface was sputtered briefly but not annealed. AES showed residual oxygen on the surface with typical O/Ti atomic ratios of ~0.4. Since decomposition is a bulk rather than a surface phenomenon, no effort was made to further reduce the surface oxygen with continued sputter cycles. The sample was heated to 1750 K at a rate of 6.6 K/s, while monitoring desorption of N (m/e = 14), N_2 (m/e = 28), Ti (m/e = 48), and TiN (m/e = 62) with the mass spectrometer.

RESULTS

Temperature Programmed Desorption

The NH_3 TPD spectra exhibit two molecular desorption peaks, as shown in Figure 1. The higher temperature state, at ~350 K, fills first and saturates at a coverage (θ_0) of ~0.05 ML (1 ML $\equiv$ 1 NH_3/TiN, or $\approx 1\times10^{15}$ molecules/cm^2). Then the low temperature state at 140 K begins to fill and continues to grow without achieving saturation. Although it appears that the intensity of the peak at 350 K continues to increase, the rise is in fact due to the higher background level from the tail of the low-temperature peak. Background subtraction confirms the saturation of the high-temperature peak. Offsetting the spectra such that the background levels adjacent to the high-temperature peak overlap demonstrates that the magnitude of this peak is in fact constant.

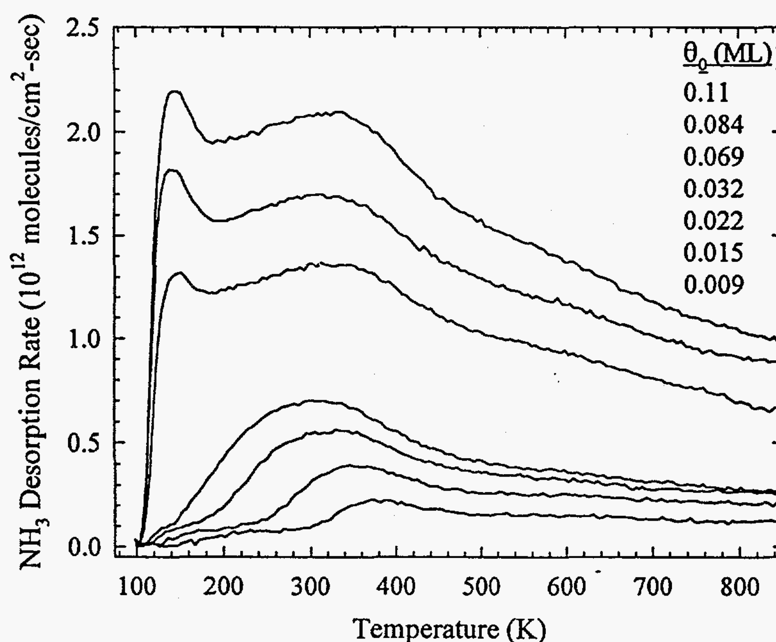

Figure 1 Temperature programmed desorption spectra of increasing coverages of NH_3 from TiN. θ_0 = 0.009, 0.015, 0.022, 0.032, 0.069, 0.084, and 0.11 ML, from bottom to top.

Other species were monitored during the temperature ramps, including N_2, H_2, and H_2O. During some experiments, H_2 desorption was detected. The peak was not reproducible, however, and may be due to desorption from the sample mounts. H_2 could also be a product of NH_3 dissociation, but in that case it would likely be accompanied by desorption of N_2, which was not detected. It is possible that small amounts of nitrogen remain on the surface and are incorporated into the TiN lattice, particularly in locally nitrogen-deficient regions. NH_3 dissociation can therefore not be completely ruled out, but since the H_2 desorption does not correlate with sample preparation or with NH_3 exposure, it is more likely attributed to an experimental artifact.

Both peaks have a long tail on the high temperature side. In the case of NH_3 desorption from GaAs(100),[29,30] a similar tail was attributed to desorption of NH_3 generated from recombination of adsorbed NH_2 with adsorbed H atoms. In order to distinguish between a high-temperature desorption feature and pumping effects, TPD experiments were performed in which the heating ramp was aborted at either 400 or 550 K, while continuing to record the mass-spectrometer signal as the sample cooled. If the high-temperature signal is due to a desorption feature, it should exhibit a sharp decrease when the heating is aborted and the peak should reappear during subsequent heating to higher temperatures. On the other hand, if the high-temperature signal is simply due to continued pumping of NH_3 that has desorbed in the lower-temperature peaks, then the temperature profile of the sample beyond the desorption peaks should not affect the mass spectrometer signal. As seen in Figure 2, there is no break in the spectrum when the sample heater is turned off. Also, no desorption is detected when the sample is later heated to 850 K. This confirms the attribution of the high-temperature tail to the slow pumping speed of NH_3. There is thus no evidence for recombinative desorption of NH_3 from TiN.

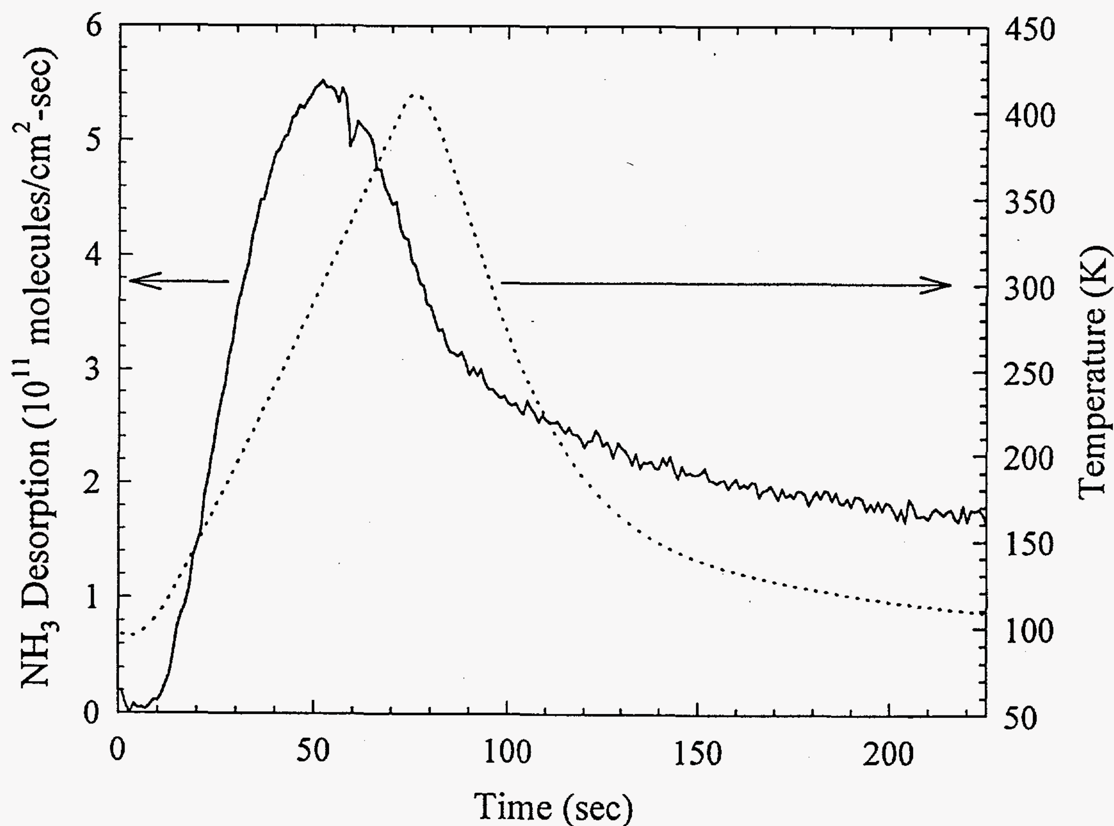

Figure 2 Temperature profile (dotted line) for an aborted TPD ramp and corresponding NH_3 desorption (solid line) as a function of time.

Sticking Probability

Two methods were used to determine the sticking probability of NH_3 on TiN. In the first method, the sticking probability at 100 K into the low-coverage state was calculated by comparing the incident flux to the integrated desorption flux. Absolute coverages were determined by using an ion gauge, which had been calibrated to a capacitance manometer, to calibrate the mass spectrometer signal. Only spectra with coverages below 0.05 ML, i.e., those exhibiting desorption only from the low-coverage state, were considered. As shown in Figure 3, the surface coverage increases linearly with incident flux, yielding a sticking probability of 0.06.

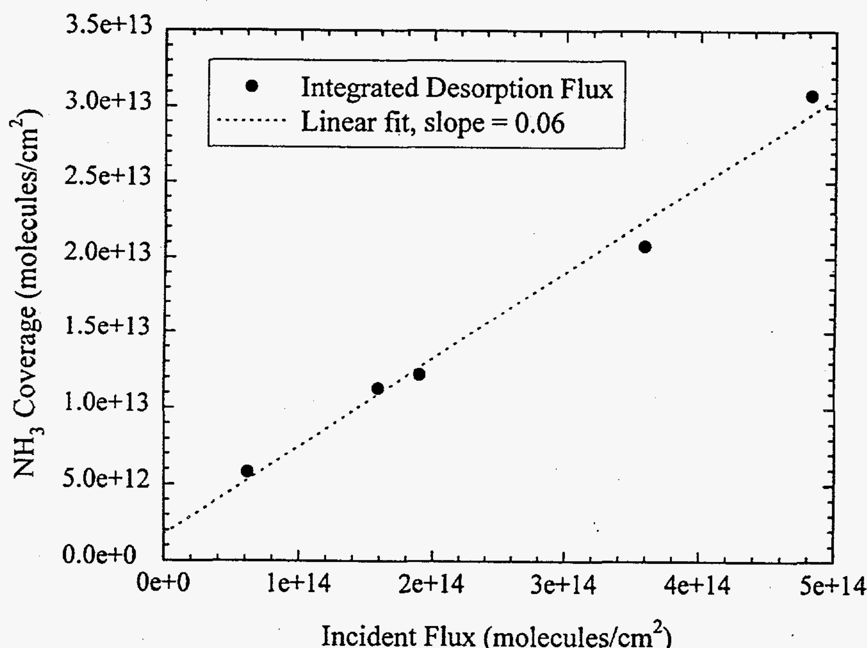

Figure 3 Surface coverage of NH_3 vs. incident flux. The slope of the line gives the sticking probability.

For the second method, the directed-beam doser technique, the surface temperature was held above the desorption temperature for the high-coverage peak. Measurements at both 150 and 200 K failed to exhibit the sharp changes in pressure described by Dresser et al.[33] since the surface was saturated with background NH_3 before being moved into the beam path. In contrast, the beam doser method determined that the sticking probability at 100 K into the low-temperature state is on the order of 1. The rapid saturation of the high-temperature state is consistent with the low value of its maximum coverage.

Decomposition of TiN

Upon heating to 1750 K in vacuum, TiN decomposes with N_2 and Ti as the only desorption products. Nitrogen is detected by the mass spectrometer at both m/e=28 and m/e=14 in a series of peaks at temperatures between 1200 and 1600 K. The shapes and locations of the peaks are not reproducible and most likely depend strongly on the history of the sample and the local

morphology of the sputtered film. No desorption is observed at m/e=12 or m/e=16 and the ratio of the m/e=14 signal to that of m/e=28 matches a reference spectrum of molecular nitrogen, confirming the identification of the desorbing species as N_2 and not CO. AES also demonstrates the removal of nitrogen from the sample between 1000 and 1750 K, as shown in Figure 4. An Auger spectrum recorded after heating to 1000 K shows the same ratio of the peak at 390 eV (due to N and Ti) to the peak at 420 eV (due to Ti) as does a freshly sputtered surface (Figure 4a). After heating to 1750 K, however (Figure 4b), the peak at 390 eV decreases due to loss of nitrogen and the 390 eV/420 eV ratio is consistent with elemental titanium (Figure 4c). Finally, the color of the sample changes from gold to silver after heating, confirming the total decomposition of TiN to Ti.

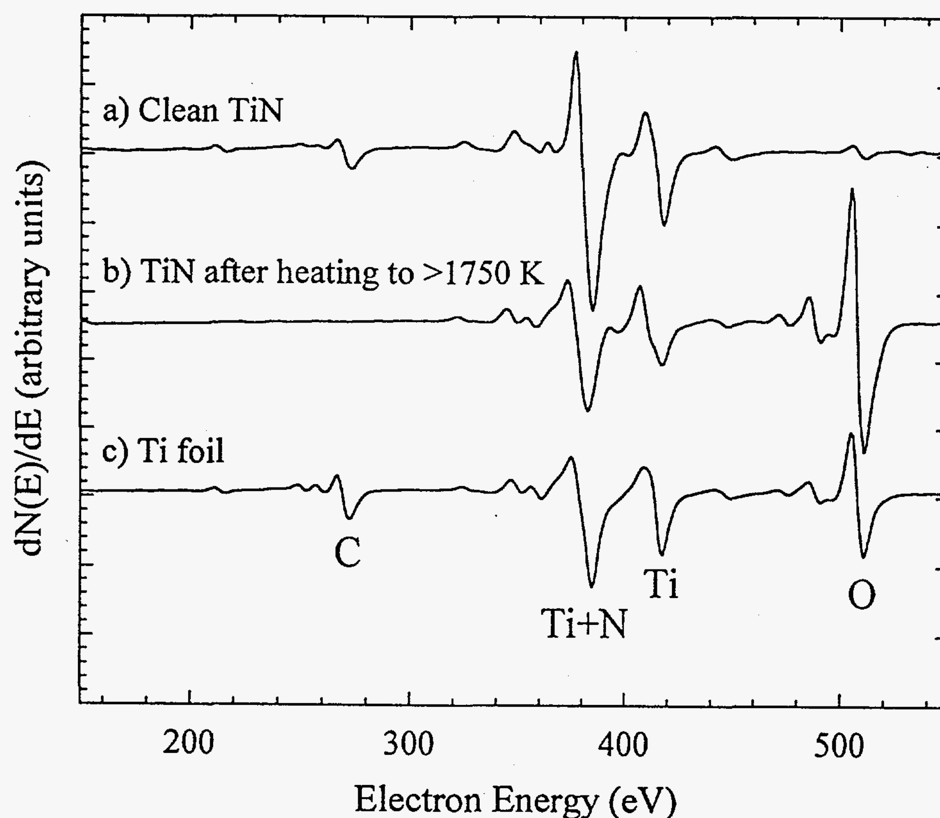

Figure 4 Auger electron spectra of a) clean TiN, b) TiN after heating to >1750 K, and c) elemental titanium foil.

Above 1600 K, atomic Ti desorbs at a rate that increases exponentially with temperature. The slope of an Arrhenius plot yields a heat of desorption of 107 kcal/mol, close to the 112.3 kcal/mol $\Delta H^{\circ}_{vaporization}$ of elemental Ti.[41] This is further evidence that the surface species remaining after the loss of nitrogen is elemental Ti and confirms the accuracy of the temperature measurement by the thermocouple.

DATA ANALYSIS

The TPD spectra were analyzed by a non-linear least-squares fitting procedure that is an extension of a previous method developed for the analysis of TPD from polycrystalline films.[42] The earlier model assumes that broad first-order desorption spectra are the result of multiple desorption sites with a Gaussian distribution of binding energies[43]. Spectra were fit to find the mean activation energy for desorption, $E_{a,m}$, and σ, the Gaussian width of the distribution, while holding the pre-exponential factor fixed at 1×10^{13} sec^{-1}. In this work, the analysis is extended by including the effect of a finite pumping speed for NH_3.

The issue of pumping speed has been discussed in general terms by Redhead.[35] The governing equation for the pressure rise in a system during a TPD experiment is:

$$\frac{dP}{dt} = -\frac{AkT}{V}\frac{d\theta}{dt} - \frac{SP}{V} \tag{2}$$

where P is pressure, t is time, A is the area of the sample, k is Boltzmann's constant, T is temperature, V is the system volume, θ is the surface coverage, and S is the pumping speed. In most TPD analyses, an infinite pumping speed is assumed ($dP/dt << SP/V$), with the result that $P \propto dq/dt$. In the case of NH_3, however, this assumption is not valid and the full equation must be utilized in the fitting procedure.

With the finite pumping speed assumption, there are two differential equations to be integrated. The first equation is the Arrhenius expression for desorption:

$$\frac{d\theta}{dt} = -\nu\theta^n \exp\left(-\frac{E_a}{RT}\right) \tag{3}$$

where ν is the pre-exponential factor, n is the reaction order, E_a is the activation energy, R is the gas constant, and the remaining parameters are as defined above. The value of $d\theta/dt$ is then substituted into Equation 2, which is integrated to obtain P.

The coefficient for the first term on the right side of Equation 2, AkT/V, is readily calculated from the geometry of the system. Its value is fixed at 8.2×10^{-23} torr-cm^2/molecule, based upon a sample area of 0.20 cm^2, a system volume of 75 l, and a temperature of 300 K. The coefficient of the second term, $\tau = V/S$, is the characteristic pumping time of the system. This becomes an additional fitting parameter and it is allowed to vary during the least-squares fitting procedure. The average value was 22 sec, although the value for each individual spectrum was dependent upon the recent history of the chamber. Independent measurements of τ provide a

consistency check for the values obtained from the fits to the desorption spectra. When a volume of NH_3 gas is admitted to the chamber, the pressure falls according to the equation

$$P(t) = P_0 e^{-t/\tau} \quad (4)$$

where P_0 is the pressure at time zero. The measured values are higher by a factor of 2 - 3 than those obtained through the fitting procedure. This discrepancy is most likely due to greater saturation of the chamber walls during the direct measurement than during a TPD experiment.

DISCUSSION

NH_3 Adsorption and Desorption

The fitting procedure just described yields an activation energy of 7.3 kcal/mol for the peak at 140 K. Since this peak is narrow, with a FWHM of < 50 K, the assumption of a Gaussian distribution of binding energies is not required, i.e., $\sigma = 0$. The higher-temperature peak is fit by considering only spectra with coverages less than 0.05 ML, where the low-temperature peak has not yet been populated. Figure 5 shows the fits to a series of low-coverage spectra following subtraction of a linear background. The peak shifts to lower temperature as θ_0 increases and $E_{a,m}$ therefore decreases from 23 kcal/mol for θ_0 = 0.003 ML to 17 kcal/mol for θ_0 = 0.03 ML. Conversely, σ increases from 2.0 to 3.5 kcal/mol through this range. A linear extrapolation suggests that $E_{a,m}$ = 24 kcal/mol in the limit of zero coverage.

A similar variation of desorption energy with coverage is observed in the NH_3/Ru(001)[23] and NH_3/NiO(100)[27] systems and is attributed to repulsive lateral interactions between the NH_3 dipoles. Such an explanation is not appropriate in the NH_3/TiN case, however. First, the coverages in question are so low (<0.05 ML) that it is unlikely that repulsive interactions play an important role in the desorption process.[44] Second, a coverage-dependent activation energy would change the shapes of the spectra significantly from that shown here, where $E_{a,m}$ is constant for each spectrum but varies according to the *initial* coverage.

An alternate explanation for the variation in $E_{a,m}$ with θ_0 arises from consideration of the fact that σ increases as $E_{a,m}$ decreases. Figure 6 shows two Gaussian distributions ($E_{a,m}$ and σ equal to 23 and 2.0 kcal/mol and 17 and 3.5 kcal/mol, respectively) with populations differing by a factor of 10, corresponding to the fit parameters for the top and bottom spectra shown in Figure 5. The upper ends of these distributions nearly coincide. This suggests that the shift in mean activation energy with initial coverage could simply result from the filling of the higher energy tail of the distribution before the lower energy end. Such a preference for the more stable states can be manifested only if there is a high mobility of NH_3 on the surface, either during the adsorption process or, more likely, as the sample is heated during the desorption experiment.

The activation energies and saturation coverages determined here can be considered in light of previous TPD studies and the bond energies of various Ti- and N-containing species to formulate a physical description of the binding states of NH_3 on TiN. Truong et al.[19] studied NH_3 desorption from TiN_x and found spectra with the same general shape as those shown in Figure 1, namely a broad peak at ~400 K, moving to lower temperatures as the coverage increases, and a sharp peak at ~125 K. Although a detailed kinetic analysis was not performed, the activation energy for desorption of the higher temperature peak was estimated to be 24 kcal/mol, in excellent agreement with the present work. On the TiO_2(001) surface,[34] NH_3 exhibits both molecular and dissociative adsorption. The molecular chemisorption state desorbs at 338 K, with an activation energy of 19 kcal/mol. On three different molybdenum nitride surfaces[25] (β-$Mo_{16}N_7$, γ-Mo_2N, and δ-MoN), NH_3 also has both molecular and dissociative adsorption states. The molecular state exhibits broad peaks at ~350 K, while the recombinative desorption features appear above 600 K. No low-temperature features were observed in either of these studies as the sample temperatures were close to 300 K during exposure to NH_3.

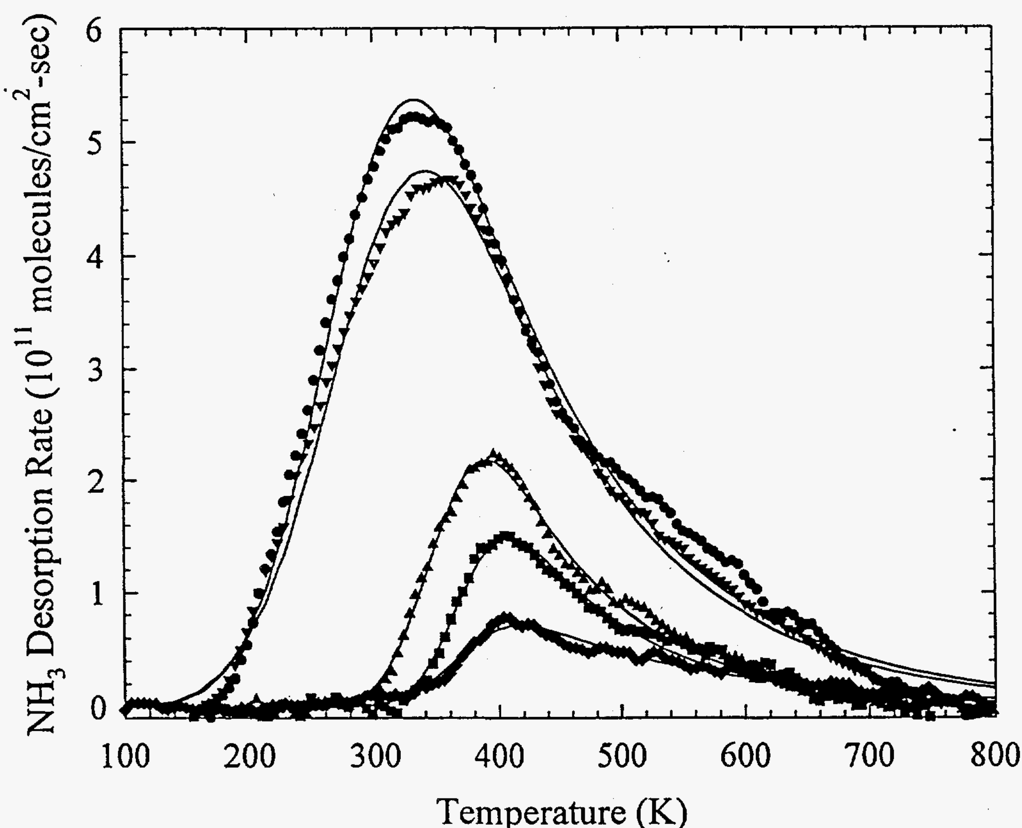

Figure 5 The low-coverage NH_3 TPD spectra (symbols) and the fits to the model (solid lines). θ_0 = 0.003, 0.006, 0.013, 0.024, and 0.026 ML, from bottom to top.

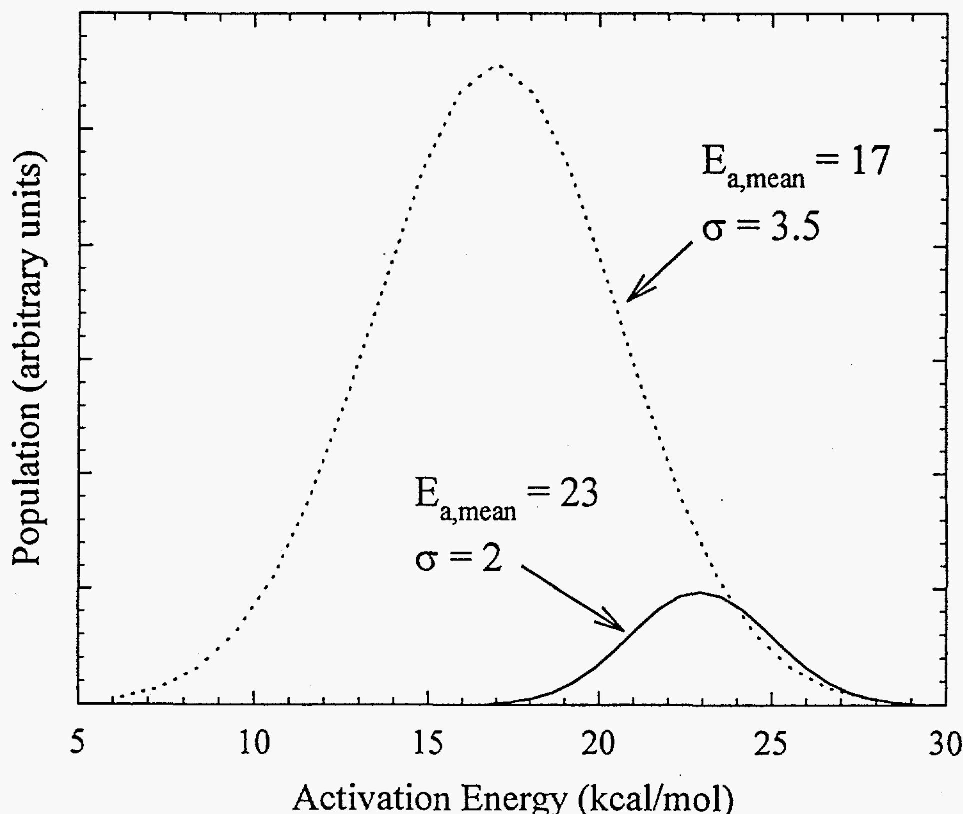

Figure 6 Comparison of two Gaussian distributions with parameters as noted and relative populations of 10:1.

In the present work, the low-temperature, high-coverage peak for NH_3 desorption from TiN does not saturate, signifying that it is a multilayer of solid NH_3. The activation energy for desorption, 7.3 kcal/mol, is similar to those found for NH_3 multilayers on Pt(111)[22] (8.6 kcal/mol) and on GaAs(100)[29] (9.8 kcal/mol), as well as to the enthalpy of physisorption of NH_3 (9.1 kcal/mol).[45] Since this peak represents interactions among NH_3 molecules rather than between NH_3 and TiN, and since its desorption temperature is far lower than temperatures characteristic of TiN CVD, it will not be considered further here.

It is more important to understand the nature of the high-temperature, low-coverage peak. The saturation coverage of 0.05 ML implies that this peak represents desorption from sites that are fairly rare on the surface, perhaps some type of defect in the TiN lattice.[46] Some insight into the nature of this site can be gained by comparing the activation energy of 24 kcal/mol with bond strengths for some related gas-phase compounds. The bond dissociation energy of gas-phase $(NH_2)_3Ti\text{-}NH_2$, an analogue of adsorbed, dissociated NH_3, has been calculated[37] as 86.1 kcal/mol. As described below, dissociation of the TiN lattice has an activation energy of at least 80 kcal/mol. The N-N bond strength in $H_2N\text{-}NH_2$ is[47] 65.8 kcal/mol. All of these are significantly higher than the desorption energy of NH_3 on TiN. Since NH_3 apparently does not dissociate on the TiN surface, a more relevant comparison is with $Cl_4Ti{:}NH_3$, in which there is a dative bond between Ti and N. The bond dissociation energy for this species is predicted by *ab initio* calculations[37] to be 17.0 kcal/mol, which is reasonably close to the 24 kcal/mol measured here. Desorption from the

molecular chemisorption state of NH_3 on $TiO_2(001)$, with E_a = 19 kcal/mol, may represent a similar process.

A physical picture for the adsorption of NH_3 on TiN can now be constructed, and this is shown in Figure 7. After sputtering and annealing the TiN surface is most likely capped with N atoms, since N is much less reactive than Ti. There may be a few locations on the surface, though, that have a different composition, perhaps a different oxidation state or coordination number. Since the TiN sample is not a single crystal, the exact nature of these sites cannot be characterized and they are represented in Figure 7a by a box around the Ti, as the chemical identity of these sites is not known. When the surface is exposed to small amounts of NH_3, it chemisorbs first at these sites, as shown in Figure 7b. The comparisons above suggest that this happens through a dative N to Ti bond, and it is desorption from this state that has an activation energy of 24 kcal/mol. When all of these sites are filled, with a saturation coverage of approximately 0.05 ML, adsorption into this state ceases. Additional NH_3 incident on the surface, Figure 7c, forms a multilayer. The multilayer, which is held together by hydrogen bonding, desorbs at ~140 K. This picture also explains why there is no separate physisorption peak for the desorption of the first layer of the solid NH_3, as there is in some other systems. The N-H bonding from the multilayer to the TiN surface is the same as that within the multilayer, so the first layer desorbs at the same temperature as the rest of the multilayer. The two peaks in the NH_3 TPD spectra therefore represent chemisorption and multilayer states.

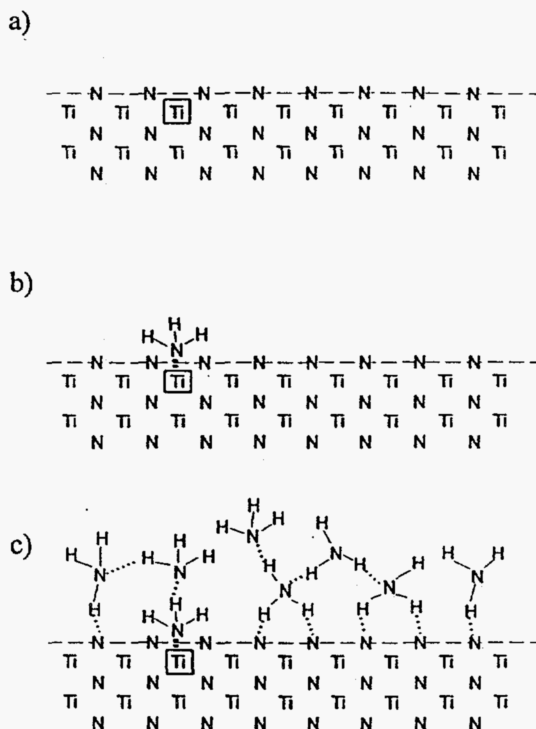

Figure 7 Proposed surface structures for NH_3 adsorption on TiN: a) annealed TiN surface, b) low coverage of NH_3, c) high coverage of NH_3

N_2 Desorption

N_2 desorbs from TiN at much higher temperatures and with more complex spectra than NH_3. Because the TPD experiment probes bulk decomposition of TiN and not surface decomposition alone, several elementary processes can contribute to the desorption profiles. These include dissociation of Ti-N bonds in bulk TiN, diffusion of nitrogen to the TiN surface, and desorption of N_2 from the surface. It is difficult to positively associate the TPD features with any of these specific rate processes without more detailed measurements and modeling. All of these kinetic processes exhibit an Arrhenius form for the temperature dependence, however, and therefore features detected between 1200 and 1600 K correspond to activation energies from 80 to 100 kcal/mol, assuming a prefactor of 10^{13} sec^{-1}. These values therefore provide an estimate of the activation energy for decomposition of TiN to Ti and N_2.

These measurements are consistent with the calculated[37] $(NH_2)_3Ti\text{-}NH_2$ bond strength of 86.1 kcal/mol, as well as with previous experimental investigations of the thermodynamics of TiN vaporization and decomposition. Hoch et al.[48] examined the vaporization of TiN in a Knudsen effusion cell and deduced that TiN decomposes into Ti(g) and N_2(g), the same products observed here, but the reaction was detected at a higher temperature (1987 K) than in the present study. This difference may be attributed to the superior sensitivity of mass spectrometry, used here to detect decomposition products, versus the weight-change method used by Hoch et al. Thus, the decomposition was detected at lower temperatures in this study.

The decomposition of TiN has also been examined with mass spectrometry by Akishin and Klodeev.[49] They report decomposition of TiN into Ti(g) and N_2(g) above 1700 K, also somewhat higher than the temperature observed here. This, too, can be attributed to the vacuum limitations of the previous work and consequent lower sensitivity that did not allow observation of the initial evolution of N_2. More recently, Lopez et al.[50] examined superlattice mixtures of TiN and NbN and found no loss of nitrogen upon heating to 973 K in a vacuum of 10^{-6} torr. Although this was not pure TiN, it supports the observation here that TiN does not decompose below 1000 K.

The behavior of nitrogen described here is fundamentally different from that observed during nitrogen adsorption measurements by You et al.[51] Using a thermal conductivity detector, a heat of adsorption of 14.6 kcal/mol was measured for N_2 on TiN powder at 900 to 950 K. This is much lower than the range of activation energies determined here for nitrogen desorption and could be energetically significant for CVD processes. However, although You et al. assumed that the N_2 dissociated upon adsorption, there is no experimental evidence for dissociation. Given the disparity between Reference 51 and the other studies, it is likely that the activation energy of 14.6 kcal/mol actually corresponds to adsorption of molecular nitrogen without dissociation.

Implications for CVD

The implications of these results for the CVD of TiN can now be considered, keeping in mind that conditions in a deposition reactor differ significantly from the UHV environment of these experiments. Total reactor pressures typically range from 150 mtorr to 760 torr, often with NH_3 mole fractions of ~10%, Ti-containing precursor mole fractions of ~1%, and the remainder consisting of carrier gases such as Ar or N_2. Substrate temperatures range from 700 - 1000 K for $TiCl_4/NH_3$ depositions and 450 - 850 K for metalorganic processes.

The activation energy for NH_3 desorption from TiN, 24 kcal/mol, is low enough that NH_3 desorbs readily at CVD temperatures. A calculation of steady-state NH_3 surface coverage as a function of substrate temperature and incident NH_3 flux shows that even under high flux conditions, the surface remains free of NH_3 and sites necessary for growth are not prevented from reacting. The sticking probability for NH_3 determined here, 0.06, is very close to the saturation coverage in the chemisorption state, 0.05 ML. This may mean that the sticking probability is actually limited by the availability of sites, i.e., the incident NH_3 molecules that land on "appropriate" sites adsorb with unit probability and the others return to the gas phase. The surface morphology and the concentration of active sites on the sputter-deposited samples used here may differ from those present under CVD conditions. As new layers of Ti and N are continually added to the lattice, it is possible that the concentration of active sites may increase and the apparent sticking probability may therefore rise. In addition, there may be other important surface processes, such as surface transamination in the metalorganic case,[19] or surface reactions with Cl-containing species in the inorganic case, that may be important during CVD. The lack of a dissociative adsorption state suggests that adsorption of other species is required for nitrogen incorporation into the films.

The molecular sticking probability of 0.06 can also be compared to a new model[36] for the overall reaction mechanism for TiN deposition from $TiCl_4$ and NH_3. A fit to experimentally-measured deposition rates yields a reactive sticking probability for NH_3 of 0.01. The fact that the molecular sticking probability is several times higher suggests that adsorption of molecular NH_3 is not the rate-limiting step to TiN CVD.

The desorption energy for N_2 from TiN, experimentally determined to be at least 80 kcal/mol, is consistent with calculated Ti to trivalent-N bond strengths in gas-phase compounds. N_2 has been proposed as a product of the TiN CVD reaction, as required to balance the change in oxidation state of the Ti. The desorption energy for N_2, though, is too high to for this process to contribute to reactions below 1000 K. This suggests that if N_2 is produced during low-temperature CVD of TiN, it occurs by a mechanism that does not involve breaking a Ti to trivalent-N bond.

SUMMARY

The surface chemistry of nitrogen-containing species on TiN has been investigated because of its relevance to TiN CVD. NH_3 plays an important role in TiN CVD processes, providing the nitrogen to the lattice, and it is therefore of interest to measure the binding energy of NH_3 on TiN. TPD spectra of NH_3 are difficult to analyze, however, due to its slow pumping speed in stainless-steel UHV chambers. A new fitting procedure that accounts for the long residence time has enabled the most in-depth analysis of NH_3 TPD data to date. Two peaks in the spectra, with activation energies of 24 and 7.3 kcal/mol, correspond to molecular chemisorption and multilayer states, respectively, with no evidence for dissociation of NH_3. The sticking probability of NH_3 on TiN is ~0.06, consistent with a new model for the overall deposition reaction. Once incorporated into the lattice, nitrogen is strongly bound to TiN. N_2 desorbs with an activation energy of at least 80 kcal/mol, in excellent agreement with the *ab initio* Ti-N bond strength[37] of 86.1 kcal/mol. This precludes N_2 production by TiN decomposition under CVD conditions.

ACKNOWLEDGMENTS

This work was supported by the Laboratory Directed Research and Development Program at Sandia National Laboratories.

REFERENCES

1. A. Intemann, H. Koerner, and F. Koch, J. Electrochem. Soc. **140**, 3215 (1993).
2. A. Sherman, Jap. J. Appl. Phys. **30**, 3553 (1991).
3. M. Wittmer and H. Melchior, Thin Solid Films **93**, 397 (1982).
4. S. R. Kurtz and R. G. Gordon, Thin Solid Films **140**, 277 (1986).
5. M. J. Buiting, A. F. Otterloo, and A. H. Montree, J. Electrochem. Soc. **138**, 500 (1991).
6. Y. Ohshita, W. Fukagawa, and A. Kobayashi, J. Crystal Growth **146**, 188 (1992).
7. M. Nadal and F. Teyssandier, J. de Physique IV, Colloque C5, supplement to J. de Physique II **5**, C5-809 (1995).
8. R. M. Fix, R. G. Gordon, and D. M. Hoffman, Chem. Mater. **2**, 235 (1990).
9. J. A. Prybyla, C.-M. Chiang, and L. H. Dubois, J. Electrochem. Soc. **140**, 2695 (1993).
10. S. C. Sun and M. H. Tsai, Thin Solid Films **253**, 440 (1994).
11. R. M. Fix, R. G. Gordon, and D. M. Hoffman, Mat. Res. Soc. Symp. Proc. **168**, 357 (1990).
12. L. H. Dubois, B. R. Zegarski, and G. S. Girolami, J. Electrochem. Soc. **139**, 3603 (1992).
13. B. H. Weiller, Mat. Res. Soc. Symp. Proc. **334**, 379 (1994); B. H. Weiller, Mat. Res. Soc. Symp. Proc. **335**, 159 (1994); B. H. Weiller and B. V. Partido, Chem. Mater. **6**, 260 (1994).
14. J. B. Everhart and B. S. Ault, Inorg. Chem. **34**, 4379 (1995).
15. J. Cueilleron and M. Charret, Bull. Soc. Chim. Fr., 802 (1956).
16. M. Antler and A. W. Laubengayer, J. Am. Chem. Soc. **77**, 5250, (1955).
17. G. W. A. Fowles and F. H. Pollard, J. Chem. Soc., 2588 (1953).
18. Y. Saeki, R. Matsuzaki, A. Yajima, and M. Akiyama, Bull. Chem. Soc. Jpn. **55**, 3193 (1982).
19. C. M. Truong, P. J. Chen, J. S. Corneille, W. S. Oh, and D. W. Goodman, J. Phys. Chem. **99**, 8831 (1995).
20. G. B. Fisher, Chem. Phys. Lett. **79**, 452 (1981).
21. J. M. Gohndrone, C. W. Olsen, A. L. Backman, T. R. Gow, E. Yagasaki, and R. I. Masel, J. Vac. Sci. Technol. **A7**, 1986 (1989).
22. J. L. Gland and E. B. Kollin, J. Vac. Sci. Technol. **18**, 604 (1981).
23. C. Benndorf and T. E. Madey, Surf. Sci. **135**, 164 (1983).
24. R. Bafrali and A. T. Bell, Surf. Sci. **278**, 353 (1992).
25. H. J. Lee, J.-G. Choi, C. W. Colling, M. S. Mudholkar, L. T. Thompson, Appl. Surf. Sci. **89**, 121 (1995).
26. C. Klauber, M. D. Alvey, and J. T. Yates, Jr., Surf. Sci. **154**, 139 (1985).
27. M.-C. Wu, C. M. Truong, and D. W. Goodman, J. Phys. Chem. **97**, 4182 (1993).
28. S. T. Ceyer and J. T. Yates, Jr., Surf. Sci. **155**, 584 (1985).
29. N. K. Singh, A. J. Murrell, and J. S. Foord, Surf. Sci. **274**, 341 (1992).

30. E. Apen and J. L. Gland, Surf. Sci. **321**, 301 (1994).

31. Y.-M. Sun, D. W. Sloan, T. Huett, J. M. White, and J. G. Ekerdt, Surf. Sci. Lett. **295**, L982 (1993).

32. P. A. Taylor, R. M. Wallace, W. J. Choyke, M. J. Dresser, and J. T. Yates, Jr., Surf. Sci. Lett. **215**, L286 (1989).

33. M. J. Dresser, P. A. Taylor, R. M. Wallace, W. J. Choyke, and J. T. Yates, Jr., Surf. Sci. **218**, 75 (1989).

34. E. Román and J. L. de Segovia, Surf. Sci. **251/252**, 742 (1991).

35. P. A. Redhead, Vacuum **12**, 203 (1962).

36. R. S. Larson and M. D. Allendorf, CVD-XIII, Proc. of the Thirteenth Intl. Conf. on Chemical Vapor Deposition (The Electrochemical Society, Pennington, NJ), in press.

37. M. D. Allendorf, C. L. Janssen, M. E. Colvin, C. F. Melius, I. M. B. Nielsen, T. H. Osterheld, and P. Ho, *Process Control, Diagnostics, and Modeling in Semiconductor Manufacturing I* (The Electrochemical Society, Pennington, NJ, 1995), Vol. **95-2**, 393.

38. M. T. Schulberg, M. D. Allendorf, and D. A. Outka, Surf. Sci. **341**, 262 (1995).

39. M. T. Schulberg, M. D. Allendorf, and D. A. Outka, Mat. Res. Soc. Symp. Proc. **410**, in press.

40. L. E. Davis, N. C. MacDonald, P. W. Palmberg, G. E. Riach, and R. E. Weber, Handbook of Auger Electron Spectroscopy, 2nd ed. (Physical Electronics Division, Perkin Elmer Corporation, Eden Prairie, MN, 1976).

41. R. C. Weast, Ed., Handbook of Chemistry and Physics, 70th ed. (CRC Press, Boca Raton, FL, 1989).

42. M. D. Allendorf and D. A. Outka, Surf. Sci. **258**, 177 (1991).

43. Briefly, the model considers a range of *N* sites on the surface with first order desorption energies E_i, where $I = 1$ to N. The total desorption rate is then

$$\frac{d\theta}{dt} = -\nu \sum_{i=1}^{N} \theta(E_i) \exp\left(-\frac{E_i}{RT}\right)$$

The initial concentration of sites with a given energy, $\theta^0(E_i)$, is given by

$$\theta^0(E_i) = P(E_i)\, \theta^0$$

where the Gaussian distribution is used for $P(E_i)$.

44. Repulsive interactions could be significant at low coverages if the adsorption sites are clustered, however.

45. D. O. Haywood and B. M. W. Trapnell, *Chemisorption* (Butterworths, London, 1964).

46. It is possible that these minority sites are related to the carbon and/or oxygen impurities on the TiN surface. No correlation was found, however, between the saturation coverage achieved and the carbon Auger signal prior to the dose. The TiN_x substrates studied in Reference 19, which displayed similar spectra, also contained substantial carbon impurities. Further experiments with higher-purity films are required to resolve this issue.

47. D. F. McMillen and D. M. Golden, Ann. Rev. Phys. Chem. **33**, 493 (1982).
48. M. Hoch, D. P. Dingledy, and H. L. Johnston, J. Amer. Chem. Soc. **77**, 304 (1955)..
49. P. A. Akishin and Y. S. Klodeev, Russ. J. Inorg. Chem. **7**, 486 (1962).
50. S. Lopez, M.-S. Wong, and W. D. Sproul, J. Vac. Sci. Technol **A13**, 1644 (1995).
51. M. S. You, N. Nakashini, and E. Kato, J. Electrochem. Soc. **138**, 1394 (1991).

INITIAL DISTRIBUTION
UNLIMITED RELEASE

Dr. Peter Angelini
Bldg. 4515
Oak Ridge National Laboratories
Oak Ridge, TN 37831-6065

Dr. Sara Dillich
Adv. Industrial Concepts Div., EE-232
U.S. DOE-EE
Forrestal Building, 1000 Independence Avenue
Washington, D.C. 20585

Dr. Charles A. Sorrell
Adv. Industrial Concepts Divs., EE-232
U.S. DOE-EE
Forrestal Building, 1000 Independence Avenue
Washington, DC 20585

Dr. Theodore M. Besmann
Oak Ridge National Laboratories
P.O. Box 2008
Oak Ridge, TN 37831-6063

Dr. Suleyman A. Gokoglu
NASA Lewis Research Center
Mail Stop 106-1
Cleveland, OH 44135

Dr. John W. Hastie
National Inst. of Standards & Technology
Metallurgy Division
B106/223
Gaitherburg, MD 20899

Dr. Gerd M. Rosenblatt
Building 50A, Room 4119
Lawrence Berkeley Laboratory
1 Cyclotron Road
Berkeley, CA 94720

Dr. Michael Zachariah
National Institute of Standards and Technology
Building 221, Rm. B312
Gaithersburg, MD 20899

Prof. Peter B. Armentrout
Department of Chemistry
University of Utah
Henry Eyring Building
Salt Lake City, UT 84112

Professor Richard Axelbaum
Dept. of Mechanical Engineering
Washington University
St. Louis, MO 63130

Prof. Dieter Baeuerle
Johannes-Kepller-Universitat Linz
Institute fur Angewandte Physik
A-4040 Linz
Austria

Prof. C. Bernard
Laboratories de Thermodynamique
ENSEEG
BP.75,38402
St. Martin d'Heres
France

Dr. Ken Brezinsky
Department of Mechanical & Aerospace Engineering
Princeton University
Engineering Quadrangle, D329
Princeton, NJ 08544

Professor Mark A. Capelli
Department of Mechanical Engineering
Stanford University
Building 500
Stanford, CA 94305

Prof. Jan-Otto Carlsson
Uppsala University
Chemistry Department
Box 531
S-75121 Uppsala
Sweden

Prof. David S. Dandy
Dept. of Agricultural and Chemical Engineering
Colorado State University
Fort Collins, CO 80523

Prof. Robert F. Davis
Dept. of Materials Science and Engineering
Virginia Polytechnic Institute
213 Holden Hall
Blacksburg, VA 24061-0140

Professor Seshu B. Desu
Dept. of Materials Science and Engineering
Virginia Polytechnick Institute
213 Holden Hall
Blacksburg, VA 24061-0140

Prof. James Edgar
Department of Chemical Engineering
Kansas State University
Manhattan, Kansas 66506-6102

Prof. James W. Evans
Dept. of Materials Science and Mineral Engineering
University of California
Berkeley, CA 94720

Prof. Richard C. Flagan
Environmental Engineering
California Institute of Technology
138-78
Pasadena, CA 91125

Prof. Arthur Fontijn
Dept. of Chemical Engineering
Pennsylvania State University
202 Academic Projects Building
University Park, PA 16802

Prof. Bernard Gallois
Dept. of Materials Science
Stevens Institute Technology
Castle Point on the Hudson
Hoboken, NJ 07030

Prof. Steven M. George
Department of Chemistry
University of Colorado
Boulder, CO 80309

Prof. David G. Goodwin
Dept. of Mechanical Engineering
and Applied Physics
California Institute of Technology
Mail Code 104-44
Pasadena, CA 91125

Professor Roy G. Gordon
Department of Chemistry
Harvard University
12 Oxford Street
Cambridge, MA 02138

Dr. Robert H. Hauge
Dept. of Chemistry
Rice University
Houston, TX 77251

Prof. Peter Hess
Institut fur Physikalische Chemie
Heidelberg University
Im Neuenheimer Feld 253
69120 Heidelberg
Germany

Professor Robert F. Hicks
Department of Chemical Engineering
University of California
5531 Boelter Hall
Los Angeles, CA 90095-1592

Prof. Michael L. Hitchman
Dept. of Pure and Applied Chemistry
University of Stratclyde
195 Cathedral Street
Glasgow G1 1XL United Kingdom

Prof. Stanislawa Jonas
Department of Ceramics
University of Mining and Metallurgy
Mickiewicza Street 30
30-059 Cracow POLAND

Prof. Linda Jones
NYS College of Ceramics
Alfred University
2 Pine Street
Alfred, NY 14802

Professor Joseph L. Katz
Chemical Engineering
Johns Hopkins University
Charles and 34th Streets
Baltimore, MD 21218

Prof. Keith King
Department of Chemical Engineering
University of Adelaide
Adelaide, SA Australia 5005

Prof. H. Komiyama
Department of Chemical Engineering
University of Tokyo
Hongo 7, Bunkyo-ku
Tokyo 113
Japan

Dr. F. Langlais
Laboratoire des Composites
Thermostructuraux
Domaine Univesitaire
33600 Pessac
France

Prof. M.C. Lin
Department of Chemistry
Emory University
Atlanta, GA 30322

Prof. Paul Marshall
Department of Chemistry
University of North Texas
P.O. Box 5068
Denton, TX 76203-5068

Prof. Triantafillos J. Mountziaris
Chemical Engineering Dept.
SUNY Buffalo
Buffalo, NY 14260

Dr. Roger Naslain
Laboratoire des Composites
Thermostructuraux
Domaine Universitaire
33600 Pessac
France

Dr. Michel Pons
Laboratoire de Science des Surfaces et
Marterizux Carbones
Institut National Polytechnique de Grenoble
ENSEEG
38402 Saint-Martin'D'heres Cedex
France

Prof. Daniel E. Rosner
Chemical Engineering Dept.
Yale University
P.O. Box 2159, Yale Station
New Haven, CT 06520-2159

Prof. Selim Senkan
Chemical Engineering Dept.
UCLA
5531 Boelter Hall, KE2R
Los Angeles, CA 900245-1592

Prof. Brian W. Sheldon
Division of Engineering
Brown University
Box D
Providence RI 02912

Dr. Daniel J. Skamser
Dept. of Materials Science and Engineering
Northwestern University
MLSF 2036
Evanston, IL 60208-3108

Prof. Stratis V. Sotirchos
Dept. of Chemical Engineering
University of Rochester
Rochester, NY 14627-0166

Prof. Karl E. Spear
Dept. of Cermic Science and Engineering
Pennsylvania State University
201 Steidle Building
University Park, PA 16802

Prof. Thomas L. Starr
Room 113
Baker Building
Georgia Institute of Technology
Atlanta, GA 30332-0245

Professor Stan Veprek
Institute of Chemistry of Information
Recording
Technical University of Munich
Lichtenbergstrasse 4
D-8046 Barching-Munich
Germany

Dr. Thomas H. Baum
Advanced Technology Materials
7 Commerce Drive
Danbury, CT 06810-4169

Dr. H.F. Calcote
Director of Research
Aerochem Research Laboratories
P.O. Box 1
Princeton, NJ 089542

Prof. Mark D'Evelyn
Department of Materials Engineering
Rensssalauer Polytechnic Institute
Troy, NY 12180

Dr. Robert Foster
CVD Division
MRC
3821 East Broadway Road
Phoenix, AZ 85040

Dr. Douglas W. Freitag
DuPont Lanxide Composites, Inc.
17 Rocky Glen Court
Brookeville, MD 20833

Dr. Jitendra S. Goela
Morton Advanced Materials
185 New Boston Street
Woburn, MA 01801-6278

Dr. Christopher J. Griffin
3M Corporation
3M Center, Building 60-1N-01
St. Paul, MN 55144-1000

Dr. Stephen J. Harris
Physical Chemistry Dept.
GM Research and Development
30500 Mound Road 1-6
Warren, MI 48090-9055

Dr. Mark H. Headinger
DuPont Lanxide Composites, Inc.
400 Bellevue Road, P.O. Box 6100
Newark, DE 19715-6100

Dr. Donald L. Hildenbrand
SRI International
AG231
333 Ravenswood Avenue
Menlo Park, CA 94025

Dr. Joseph Hillman
MRC
3821 East Broadway Road
Phoenix, AZ 85040

Dr. Robert Jackson
Novellus Systems, Inc.
81 Vista Montana
San Jose, CA 95134

Dr. James Loan
MKS Instruments, Inc.
6 Shattuck Road
Andover, MA 01810

Dr. K. L. Luthra
General Electric Corporate Research and Development
Room 3B4, Building K1
Schenectady, NY 12301

Dr. Richard J. McCurdy
Libbey-Owens-Ford Co.
1701 East Broadway
Toledo, OH 43605

Dr. Meyya Meyyappan
Scientific Research Associates
50 Nye Road
Glastonbury, CT 06033

Dr. Thomas H. Osterheld
Applied Materials, Inc.
Mail Stop 1510
Santa Clara, CA 95054

Dr. Duane A. Outka
Lam Research Corporation
Mail Stop CA3
4650 Cushing Parkway
Fremont, CA 94538

Dr. Ronald A. Powell
Varian Research Center
3075 Hansen Way
Palo Alto, CA 94303

Mr. Peter Reagan
Project Manager, CVD Composites
Thermo Trex Corporation
74 West Street, PO Box 9046
Waltham, MA 02254-9046

Dr. David Roberts
J.C. Schumacher
1969 Palomar Oaks Way
Carlsbad, CA 92009

Dr. John A. Samuels
Semiconductor Equipment Group
Watkins-Johnson Co.
440 Kings Village Road, Building 5
Scotts Valley, CA 95066-4081

Dr. Michelle Schulberg
Varian Associates
3075 Hansen Way, MS K-455
Palo Alto, CA 94304

Dr. Andrew J. Sherman
Ultramet
12173 Montague Street
Pacoima, CA 91331

Dr. Craig B. Shumaker
DuPont Lanxide Composites Inc.
1300 Marrows Road
Newark, DE 19714-6077

Dr. Richard Silberglitt
Technology Assessment and Transfer, Inc.
133 Defense Highway, #212
Annapolis, MD 21401

Dr. Brian Thomas
Naval Research Laboratory
Code 6174
4555 Overlook Avenue SW
Washington, DC 20375-5000

Dr. Bruce H. Weiller
Mechanics and Materials Technology Center
Aerospace Corporation
P.O. Box 92957
Los Angeles, CA 9009-2957

MS0349 S.T. Picraux, 1112

MS0601 W.G. Breiland, 1126

MS0601 M.E. Coltrin, 1126

MS0601 P. Esherick, 1126

MS0601 P. Ho, 1126

MS1349 R.E. Loehman, 1808

MS1393 D.W. Schaefer, 1814

MS0457 R.J. Eagan, 5600

MS0702 D.E. Arvizu, 6200

MS0710 G.A. Carlson, 6211

MS9003 T.O. Hunter, 8000
Attn: 8200 R.J. Detry
8400 L.A. Hiles

MS9214 C.F. Melius, 8117

MS9056 W.J. McLean, 8300
Attn: 8302 W. Bauer
8351 L. Rahn
8362 R. Carling
8366 B. Gallagher

MS9161 R.H. Stulen, 8342

MS9042 C.M. Hartwig, 8345
Attn: E. Evans
S. Griffiths
W.G. Houf
R. Nilson

MS9161 D.A. Outka, 8347

MS9162 A.E. Pontau, 8347

MS9055 F.P. Tully, 8353

MS9052 M.D. Allendorf, 8361 (10)

MS9052 D.R. Hardesty, 8361 (5)

MS9401 M.T. Dyer, 8700
Attn: 8711 M.W. Perra
8712 M.I. Baskes
8713 J.C.F. Wang
8715 G.J. Thomas
8716 K.L. Wilson
8717 W.G. Wolfer

MS9042 R.J. Kee, 8745

MS9042 R. Larson, 8745

MS9042 E. Meeks, 8745

MS9021 Technical Communications Department, 8535, for OSTI (10)

MS9021 Technical Communications Department, 8535/Technical Library, MS0899, 13414

MS0899 Technical Library, 13414 (4)

MS9018 Central Technical Files, 8523-2 (3)